

Surface plasmon resonances of single and coupled metallic nanoparticles: A boundary integral method approach

Ulrich Hohenester* and Joachim Krenn

Institut für Physik, Karl-Franzens-Universität Graz, Universitätsplatz 5, 8010 Graz, Austria

(Received 10 June 2005; revised manuscript received 26 August 2005; published 28 November 2005)

We employ the boundary integral method for the calculation of plasmon resonances in single and coupled metallic nanoparticles. A generic and versatile scheme is developed that allows us to compute the optical properties of arbitrarily shaped nanoparticles embedded in dielectric environments with complex geometry. In the static limit an eigenvalue problem is formulated whose solutions directly provide the plasmon resonances. We present results for spherical, cylindrical, and cubic particles, and discuss the role of coupling and retardation.

DOI: [10.1103/PhysRevB.72.195429](https://doi.org/10.1103/PhysRevB.72.195429)

PACS number(s): 73.20.Mf, 71.45.Gm, 41.20.-q

I. INTRODUCTION

Noble-metal nanoparticles can interact strongly with visible light due to the resonant excitation of surface plasmon modes. These modes are characterized by spectrally selective absorption and scattering, and give rise to an enhancement of the local field with respect to the exciting light field.¹ A variety of applications are based on these effects, such as surface-enhanced Raman scattering,^{2,3} biochemical detection,⁴ or optical addressing of subwavelength volumes.⁵ Of specific interest is the electromagnetic interaction of two or more nanoparticles in close proximity to one another. Such configurations give rise to tunable spectral shifts of the plasmon bands and to exceptionally strong field enhancements.^{6,7} Indeed, the general interest in this field has strongly increased in recent years as improved nanofabrication methods now allow advanced control of nanoparticle shape and arrangement patterns of particle ensembles. It is evident that this advancement has to be complemented by accordingly powerful computational schemes.

In the theoretical description of the optical response of metallic nanoparticles with arbitrary shape one usually employs the finite difference time domain (FDTD)⁸⁻¹⁰ or the dyadic Green-function technique.¹¹ Within the latter approach, the volume of the nanoparticle is discretized into small volume elements. The linear response to an external field is then obtained by computing the response of each volume element to the total field, produced by the external probe and the polarization of all other elements, and putting together the responses of all volume elements. Here, the action from one volume element to another one is mediated by the dyadic Green function. This allows to incorporate effects of nontrivial dielectric environments of the nanoparticles, such as surfaces¹² or multilayers,¹³ by choosing the corresponding Green functions. Contrary to the FDTD technique, whose computational complexity is of the order N of the number of discretization elements, the complexity of the Green-function approach is of the order N^3 . Accurate solutions for high-permittivity scatterers can thus only be obtained for small nanoparticles with sufficiently simple shapes.¹⁴

A substantial simplification of the Green-function approach can be achieved for nanoparticles with homogeneous

dielectric properties, i.e., when the dielectric function $\epsilon(\mathbf{r}) = \epsilon_0$ is constant within the volume of the nanoparticle (ϵ_0 might still be frequency dependent). In this case, one can convert the volume integration of the dyadic Green-function approach to a surface integration. This approach has the advantage that, instead of discretizing the complete volume of the particle, one only has to discretize the particle surface, which allows for much finer discretizations and more accurate results. Different implementations of such boundary integral method approaches exist, which are either based on Green's second theorem that directly relates the volume integration to a surface integration (direct methods),^{15,16} or on an *ad hoc* solution with some auxiliary quantities which are chosen such that the appropriate boundary conditions are fulfilled (indirect methods).^{17,18} Advantages and disadvantages of the different methods have been discussed in the literature.^{19,20}

In this paper we employ the boundary-integral-method approach for computing the optical properties of metallic nanoparticles of arbitrary shape. To this end, we approximate the particle surface by a set of triangles. For the calculation of the retarded response, we directly follow the approach presented in Refs. 17 and 18 where the boundary conditions imposed by Maxwell's equation are accounted for through auxiliary surface charges and currents (indirect method). For the nonretarded limit, we show that in case of a simplified Drude-like dielectric description the problem can be mapped onto an eigenvalue problem, whose solutions directly provide the plasmon energies and eigenfunctions (direct method). We show that such approach is particularly useful in visualizing the surface plasmon resonances of single and coupled particles.

Our paper has been organized as follows. In Sec. II we develop our theoretical scheme. We present the essential ingredients of the direct and indirect boundary integral method approach. We briefly outline the calculation scheme for the retarded case,^{17,18} discuss in more detail our approximation scheme for the nonretarded case, and present details of our computational approach. In Sec. III we demonstrate the accuracy of our computational scheme, and present results for spherical, cylindrical, and cubic nanoparticles. The role of retardation and interparticle coupling will be discussed. Finally, in Sec. IV we draw some conclusions.

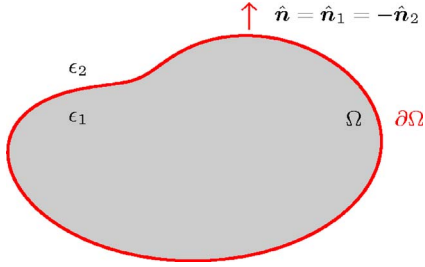


FIG. 1. (Color online) Schematic representation of the elements involved in the boundary integral method approach. The shaded region represents the metal nanoparticle, described by the (frequency dependent) dielectric constant ϵ_1 and the particle volume Ω , which is embedded in a medium of dielectric constant ϵ_2 . $\hat{\mathbf{n}}_1 = \hat{\mathbf{n}}$ ($\hat{\mathbf{n}}_2 = -\hat{\mathbf{n}}$) is the outer surface normal of medium 1 (2), and $\partial\Omega$ denotes the nanoparticle boundary.

II. THEORY

A. Boundary integral method

The problem considered in this section is the solution of the free Helmholtz equation

$$[\nabla^2 + k^2\epsilon(\mathbf{r})]\phi(\mathbf{r}) = 0, \quad (1)$$

with $\epsilon(\mathbf{r})$ the space and possibly frequency dependent dielectric function ($\mu=1$ throughout), k the photon wave vector in vacuum, and $\phi(\mathbf{r})$ the scalar potential. Although not discussed explicitly, all conclusions drawn below also apply to the Helmholtz equation for the vector potential. To be more specific, we suppose that space can be decomposed into different regions Ω_j within which the dielectric function $\epsilon(\mathbf{r}) = \epsilon_j$, $\mathbf{r} \in \Omega_j$, is constant (see Fig. 1). Depending on the choice of Ω_j , this approach allows for the description of metal nanoparticles embedded in a dielectric matrix or deposited on a substrate. The description of the metal response in terms of a constant and local dielectric function limits our approach to nanoparticles with extensions substantially larger than the inverse of the Fermi wave vector,^{21,22} and is expected to fail for small metal clusters²³ or particles with sharp edges or corners. We next introduce the Green functions $G_j(\mathbf{r}, \mathbf{r}')$ defined through

$$(\nabla^2 + k_j^2)G_j(\mathbf{r}, \mathbf{r}') = -4\pi\delta(\mathbf{r} - \mathbf{r}'), \quad \mathbf{r}, \mathbf{r}' \in \Omega_j, \quad (2)$$

subject to appropriate boundary conditions, where $k_j^2 = k^2\epsilon_j$. In this paper we shall exclusively consider the homogeneous case with $G_j(\mathbf{r}, \mathbf{r}') = \exp(ik_j|\mathbf{r} - \mathbf{r}'|)/|\mathbf{r} - \mathbf{r}'|$, though other cases, such as Green functions for surfaces or stratified media,^{11,12} could be introduced in a straightforward manner. In the sequel we describe two solution schemes of the Helmholtz equation by means of the Green function G_j , which we shall refer to as direct and indirect ones. They will be respectively employed in the solution of the nonretarded and retarded Maxwell equations.

1. Direct method

The primary idea of the direct method is to combine Eqs. (1) and (2) such that $\phi(\mathbf{r})$, $\mathbf{r} \in \Omega_j$, can be computed from the knowledge of ϕ and its surface derivative at the boundary

$\partial\Omega_j$ solely. After some elementary manipulations of Eqs. (1) and (2) one arrives by use of Green's second theorem at¹⁵

$$4\pi\phi(\mathbf{r}) = \int_{\partial\Omega_j} ds' \hat{\mathbf{n}}_j(s') \cdot [G_j(\mathbf{r}, s')\nabla_{s'}\phi(s') - \phi(s')\nabla_{s'}G_j(\mathbf{r}, s')], \quad (3)$$

with $\hat{\mathbf{n}}_j(s)$ the outer surface normal. The task to determine ϕ and its surface derivative at the boundary is usually accomplished in two steps. First, one performs the limit $\mathbf{r} \rightarrow s$, $s \in \partial\Omega_j$, in Eq. (3). As discussed in some length in Ref. 18, the normal derivative of the Green function at $s \rightarrow s'$ has to be treated with care, and one obtains

$$2\pi\phi(s) = \int_{\partial\Omega_j} ds' \hat{\mathbf{n}}_j(s') \cdot [G_j(s, s')\nabla_{s'}\phi(s') - \phi(s')\nabla_{s'}G_j(s, s')]. \quad (4)$$

In a second step, this integral equation for $\phi(s)$ is combined with the boundary conditions imposed by Maxwell's equations to obtain $\phi(s)$ and $\hat{\mathbf{n}}_j(s) \cdot \nabla_s \phi(s)$ at $\partial\Omega_j$. Once these quantities are determined, Eq. (3) allows us to compute $\phi(\mathbf{r})$ everywhere in $\mathbf{r} \in \Omega_j$. We shall return to this approach in the discussion of the nonretarded optical response.

2. Indirect method

The indirect method is different in philosophy. The solution of the Helmholtz equation (1) is written in the *ad hoc* form^{17,18}

$$\phi(\mathbf{r}) = \phi_j^e(\mathbf{r}) + \int_{\partial\Omega_j} ds' G_j(\mathbf{r}, s')\sigma_j(s'), \quad \mathbf{r} \in \Omega_j, \quad (5)$$

with $\phi_j^e(\mathbf{r})$ a solution of the free Helmholtz equation and $\sigma_j(s)$ a surface charge. By construction, the solution (5) satisfies the free Helmholtz equation everywhere except at the boundary $\partial\Omega_j$, and the surface charge σ_j has to be chosen such that the boundary conditions imposed by Maxwell's equations are fulfilled. As there is some arbitrariness in the choice of the external potential $\phi_j^e(\mathbf{r})$, the surface charge is not uniquely defined.¹⁸ For that reason, $\sigma_j(s)$ in Eq. (5) should be understood as a mathematical device rather than a physical quantity.

We now have all ingredients at hand to compute the electromagnetic response of metal nanoparticles. Quite generally, the choice whether to use the direct or indirect method in the solution of Maxwell's equation is a matter of taste. In this work we employ the indirect method in the retarded case and the direct method in the nonretarded case, essentially for the following reasons. First, in the retarded case the indirect method has the advantage that the surface charge and each component of the surface current, which is required to account for the boundary conditions of the vector potential, can be computed separately.^{17,18} Thus in a computational approach only matrices of dimension N rather than $3N$ have to be manipulated. On the other hand, in the nonretarded case we use the direct method because it allows for an interpretation of the surface charge in physical terms. This will prove

helpful in deriving an eigenvalue problem for the surface charge excitations.

B. Retarded case

Let us first consider the most general case where Maxwell's equations are solved without further approximation. In our approach we directly follow Refs. 17 and 18. For the sake of completeness, we sketch the basic ingredients of the theory and refer the interested reader for further details to the literature.^{17,18} First, the electric and magnetic fields $\mathbf{E}(\mathbf{r})$ and $\mathbf{B}(\mathbf{r})$ are expressed within the respective domains $\mathbf{r} \in \Omega_j$ in terms of the scalar and vector potentials $\phi_j(\mathbf{r})$ and $\mathbf{A}_j(\mathbf{r})$ as

$$\mathbf{E}(\mathbf{r}) = ik\mathbf{A}_j(\mathbf{r}) - \nabla\phi_j(\mathbf{r}), \quad \mathbf{B}(\mathbf{r}) = \nabla \times \mathbf{A}_j(\mathbf{r}), \quad (6)$$

where $\phi_j(\mathbf{r})$ and $\mathbf{A}_j(\mathbf{r})$ fulfill the free Helmholtz equation (1) and are related through the Lorentz gauge condition $\nabla \cdot \mathbf{A}_j(\mathbf{r}) = ik\epsilon_j\phi_j(\mathbf{r})$. We suppose that the metal is described by a complex-valued dielectric function and no free carriers are present. The general solutions are then of the form

$$\phi_j = \phi_j^e + G_j\sigma_j, \quad \mathbf{A}_j = \mathbf{A}_j^e + G_j\mathbf{h}_j, \quad (7)$$

with \mathbf{h}_j a surface current vector. Here we have introduced a compact matrix notation for the convolutions in space. The unknown quantities σ_j and \mathbf{h}_j , $j = 1, 2$, have to be determined from the boundary conditions of Maxwell's equations, i.e., the continuity of the magnetic field, of the tangential component of the electric field, and of the normal component of the dielectric displacement. Within this scheme one obtains a set of eight coupled equations, whose solutions provide the unknown surface charges and currents.¹⁸ In the following we set $\phi^e = 0$ and assume for the external vector potential a plane wave with well-defined polarization.

C. Nonretarded case

When the inverse of k_j is much smaller than the extension of the nanoparticle, one can replace the Green function by its static limit $G(\mathbf{r}, \mathbf{r}') = 1/|\mathbf{r} - \mathbf{r}'|$. We shall refer to this approximation as nonretarded. Within the indirect boundary integral method approach of Ref. 18 an eigenvalue problem can be derived, whose solutions allow the calculation of the optical properties of metallic nanoparticles such as nanorings,¹⁸ nanorods,²⁴ or nanocubes.²⁵ In this work we introduce a further approximation and assume a dielectric function of Drude form^{1,21}

$$\epsilon(\omega) = \epsilon_0 - \frac{4\pi n_0}{\omega(\omega + i\gamma_0)}, \quad (8)$$

with ϵ_0 a static dielectric constant accounting for the contribution of bound electrons to the polarizability, n_0 the metal electron density, and γ_0 the electron relaxation rate (we use gauss and atomic units, $e = m = \hbar = 1$, throughout). As we shall show next, within this Drude framework it is possible to establish a microscopic description of the electron dynamics in the metal, and to obtain an equation of motion for the nanoparticle charge excitations whose solutions can be interpreted in simple physical terms.

TABLE I. Parameters used in this work for the calculation of the Drude dielectric function (8) for gold. The electron-gas parameter r_s is related to the density through $n_0 = 4\pi r_s^3/3$ (atomic units).

Parameter	Symbol	Value
Background dielectric constant	ϵ_0	10
Electron-gas parameter	r_s	3
Inverse relaxation rate	γ_0^{-1}	10 fs

For the parameters of the Drude dielectric function (8) we use the values listed in Table I which are representative for gold. The relatively large value for ϵ_0 is due to the pronounced d -band density of states close to the Fermi energy.²⁷ A comparison of the Drude dielectric function (8) with the experimental data of Johnson and Christy²⁸ reveals a very good agreement for photon energies below 2 eV, whereas at higher energies transitions of electrons from the d bands to the conduction band lead to a substantial modification with respect to the simple Drude model.

Instead of using the Drude form (8) directly, we can also describe the metal in terms of a jellium model²³ with free electrons moving in a material with dielectric constant ϵ_0 . As shown in Appendix A, within such an approach we obtain in linear response for an external excitation \mathbf{E}_{ext} with frequency ω the equation of motion for the surface charge,

$$\omega(\omega + i\gamma_0)\sigma - M\sigma = -n_0\hat{\mathbf{n}} \cdot \mathbf{E}_{\text{ext}}, \quad (9)$$

with the matrix

$$M = 4\pi G^{-1}(2\pi + F)\{2\pi(\epsilon_0 + \epsilon_b) + (\epsilon_0 - \epsilon_b)F\}^{-1}G \quad (10)$$

accounting for the mediation of the force exerted by the complete surface charge distribution. Here, ϵ_0 is the metal background dielectric constant, ϵ_b is the dielectric constant of the surrounding medium,²⁹ $G(\mathbf{s}, \mathbf{s}')$ is the static limit of the Green function, and $F(\mathbf{s}, \mathbf{s}') = -\hat{\mathbf{n}} \cdot (\mathbf{s} - \mathbf{s}')/|\mathbf{s} - \mathbf{s}'|^3$ is its surface derivative. A convenient way to solve Eq. (9) is by computing the eigenvalues and eigenvectors of the matrix M through

$$Mu_\lambda = \omega_\lambda^2 u_\lambda. \quad (11)$$

Since M is Hermitian, the eigenvalues ω_λ^2 are real and the eigenmodes u_λ form a complete set. We can thus expand σ in terms of the u_λ , and obtain for the solution of Eq. (9) the simple expression

$$\sigma = -n_0 \sum_\lambda \frac{u_\lambda(\hat{\mathbf{n}} \cdot \mathbf{E}_{\text{ext}})}{\omega(\omega + i\gamma_0) - \omega_\lambda^2} u_\lambda \quad (12)$$

which allows us to compute the response of the nanoparticles for arbitrary perturbations \mathbf{E}_{ext} . It is important to realize that the complete spectrum of surface charge excitations is obtained through a single diagonalization of M , and that the eigenvalues ω_λ^2 and functions u_λ describe the genuine excitations of metal nanoparticles. For that reason, we shall refer to them as the *surface plasmon* energies and eigenmodes. They often allow for a particularly simple and intriguing physical interpretation. In comparison to the eigenvalue

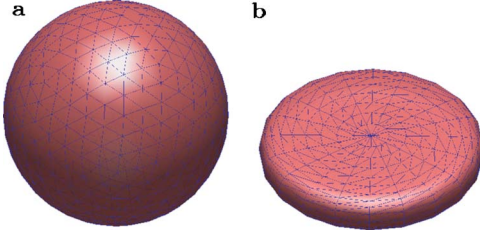


FIG. 2. (Color online) Shape of metal nanoparticles studied in this work: (a) sphere and (b) cylinder with diameter-to-height ratio of 6:1. The shapes are approximated by a set of 796 and 760 triangles (faces), respectively.

problem of the indirect boundary integral method approach,^{18,25,26} our scheme has the advantage that the eigenenergies directly provide the surface plasmon energies and that the eigenmodes can be interpreted as the surface charge densities of the jellium model. On the other hand, its limitation is the validity of the Drude description (8) which may fail in some cases, where the indirect approach²⁶ becomes superior because it allows us to cope with generic dielectric functions.

D. Computational scheme

In our computational scheme we start by approximating the boundary $\partial\Omega$ of the metal nanoparticles by a set of triangles using a standard Delaunay triangulation scheme³⁰ (Fig. 2). Within each face of the triangulated surface we approximate the surface charges σ_j (or, in the nonretarded case, σ) and currents \mathbf{h}_j as constant. These piecewise constant parts of σ and \mathbf{h} are connected through the surface Green functions G_j and surface derivatives F_j ,

$$G_j(\mathbf{s}, \mathbf{s}') = \frac{e^{ik_j s}}{s},$$

$$F_j(\mathbf{s}, \mathbf{s}') = -\hat{\mathbf{n}}(\mathbf{s}') \cdot \hat{\mathbf{e}}(ik_j s - 1) \frac{G_j(\mathbf{s}, \mathbf{s}')}{s}, \quad (13)$$

with $s = |\mathbf{s} - \mathbf{s}'|$ the distance and $\hat{\mathbf{e}} = (\mathbf{s} - \mathbf{s}')/s$ the unit vector. A computationally more simple scheme is obtained by replacing the $1/s$ terms in Eq. (13) by the softened $1/\sqrt{s^2 + s_0^2}$ ones, where s_0 is of the order of the discretization length Δx (defined as the square root of the mean area of the triangles). More specifically, in this work we set $s_0 = \Delta x/64$. This soft function has the advantage that integrations involving Green functions can be performed more easily, and the error introduced is of the same order as that of the discretization. The Green functions connecting triangles i and j are obtained from Eq. (13) as follows: if the distance s_{ij} is sufficiently small, say $s_{ij} < 6\Delta x$, the integration over triangles i and j is performed numerically; otherwise, we replace s and \mathbf{s}' by the center coordinates \mathbf{s}_i and \mathbf{s}_j of the triangles. In all cases, we approximate the phase factors e^{iks} by $e^{iks_{ij}}$. This has the advantage that the computationally costly triangle integrations have to be performed only once.

III. RESULTS

In this work we investigate surface plasmon modes for the spherical and cylindrical nanoparticles depicted in Fig. 2, and for cubic particles (see discussion below). For the sphere discretization we use a special set of points,³¹ which was obtained by minimizing the potential Coulomb energy of a set of point charges on the surface of the unit sphere. For the cylinders, we start from a sphere with radius r_0 , where the azimuthal and polar angles are discretized in equidistant meshes, and scale the z component according to $z(r) = z_0 \tanh \beta [1 - (r/r_0)^2]^{1/2} / (2 \tanh \beta)$. Here, z_0 is the height of the cylinder and β a constant that is chosen such that the radius of curvature at $z=0$ equals z_0 . This procedure yields cylinderlike particles whose edges are rounded off. Throughout we use a diameter-to-height ratio of 6:1.

A. Convergence and accuracy

The eigenvalue problem (11) for a sphere can be solved analytically within Mie theory, and one obtains for $\epsilon_0 = \epsilon_b = 1$

$$\omega_\ell^2 = \frac{\ell}{2\ell + 1} \omega_{\text{pl}}^2, \quad (14)$$

with ℓ the angular momentum of the plasmon mode and $\omega_{\text{pl}} = (4\pi n_0)^{1/2}$ the plasma frequency. The corresponding eigenfunctions with degeneracy $2\ell + 1$ are given by the spherical harmonics $Y_{\ell m}(\theta, \phi)$. In the following we use these results to test the accuracy of our computational scheme. Table II shows a comparison of our computed results with the analytic ones for different discretizations of the triangulated surface. Throughout, the discretization error is of the order of maximally a few percent and decreases monotonically with an increasing number of triangles (faces). The values in parentheses report the standard deviations for the degenerate eigenstates, which are negligible throughout.³² From the comparison of the results obtained with and without triangle integration (see different columns in Table II), we find that triangle integration is essential in order to obtain converged and quantitatively correct results.

B. Single nanoparticles

We next turn to the discussion of the surface plasmon modes for gold nanoparticles, described by the Drude-like dielectric function (8), which are embedded in a homogeneous matrix with dielectric constant $\epsilon_b = 2.25$. In doing so, we use the plasmon eigenmodes computed within our nonretarded approach to discuss the general features of such modes, and employ the retarded approach suited for the full solution of Maxwell's equations to compute the optical spectra. Figure 3 shows the plasmon eigenmodes for a sphere as computed within our nonretarded eigenvalue approach (Sec. II C). Indeed, the eigenfunctions exhibit the expected s, p , and d -like symmetries of the spherical harmonics $Y_{\ell m}(\theta, \phi)$. The corresponding energies are reported in the figure caption. A word of caution is at place since the plasmon energies are above the threshold for d -band transitions in gold, and

TABLE II. Comparison of the results of our computational scheme with the analytic result (14) for a sphere and for $\epsilon_0 = \epsilon_b = 1$. We set $n_0 = 1$. The deviation $\Delta\omega_\ell$ from the exact result is shown for different numbers of triangles (faces) and different values of ℓ , and for the case where the matrices G_{ij} and F_{ij} are obtained by integration over triangles i and j (i.e., with triangle integration) or by approximating them with $G(s_i, s_j)$ and $F(s_i, s_j)$ (i.e., without triangle integration), where s_i and s_j are the center coordinates of triangles i and j , respectively. The values in parentheses correspond to the standard deviations of the degenerate eigenvalues.

No. vertices	No. faces	$\Delta\omega_0^2$	With triangle integration			Without triangle integration		
			$\Delta\omega_1^2$	$\Delta\omega_2^2$	$\Delta\omega_0^2$	$\Delta\omega_1^2$	$\Delta\omega_2^2$	
144	284	-0.0342	0.0380 (0.0020)	0.0801 (0.0033)	0.3267	0.3806 (0.0018)	0.3898 (0.0020)	
169	334	-0.0305	0.0310 (0.0011)	0.0668 (0.0024)	0.3074	0.3533 (0.0018)	0.3611 (0.0029)	
196	388	-0.0277	0.0250 (0.0014)	0.0558 (0.0028)	0.2888	0.3282 (0.0015)	0.3352 (0.0028)	
225	446	-0.0249	0.0207 (0.0009)	0.0472 (0.0016)	0.2728	0.3072 (0.0010)	0.3132 (0.0017)	
256	508	-0.0226	0.0171 (0.0000)	0.0400 (0.0015)	0.2579	0.2880 (0.0000)	0.2934 (0.0016)	
289	574	-0.0204	0.0145 (0.0004)	0.0345 (0.0007)	0.2451	0.2717 (0.0004)	0.2765 (0.0007)	
324	644	-0.0184	0.0125 (0.0004)	0.0299 (0.0006)	0.2334	0.2572 (0.0004)	0.2615 (0.0006)	
361	718	-0.0166	0.0108 (0.0003)	0.0262 (0.0005)	0.2228	0.2442 (0.0003)	0.2481 (0.0005)	
400	796	-0.0152	0.0093 (0.0000)	0.0229 (0.0005)	0.2128	0.2320 (0.0000)	0.2356 (0.0005)	
441	878	-0.0142	0.0079 (0.0003)	0.0199 (0.0005)	0.2032	0.2206 (0.0003)	0.2239 (0.0003)	
484	964	-0.0129	0.0070 (0.0001)	0.0177 (0.0002)	0.1951	0.2110 (0.0000)	0.2139 (0.0002)	
529	1054	-0.0119	0.0062 (0.0002)	0.0158 (0.0003)	0.1873	0.2018 (0.0002)	0.2045 (0.0003)	
576	1148	-0.0110	0.0055 (0.0001)	0.0142 (0.0002)	0.1803	0.1936 (0.0001)	0.1961 (0.0002)	
625	1246	-0.0101	0.0050 (0.0001)	0.0128 (0.0002)	0.1738	0.1861 (0.0001)	0.1884 (0.0002)	

the dielectric description of Eq. (8) is somewhat questionable. However, it turns out that the results for the experimental dielectric function of Ref. 28 are very similar, and we shall thus stick for conceptual simplicity to the Drude description (and keep in mind that one has to be cautious when comparing with experiment). Figure 4 shows the plasmon eigenmodes for cylindrical nanoparticles. The states exhibit cylinder symmetry, and all excited states are twofold degenerate. In comparison to the spheres, the eigenenergies given in the figure caption are substantially redshifted and fall into a spectral region where the Drude dielectric function can be safely used. The energies become further redshifted when the diameter-to-height ratio is further increased.

In Fig. 5 we show the scattering cross sections for different nanoparticle diameters, which we compute within our retarded boundary integral method approach (Sec. II B) and

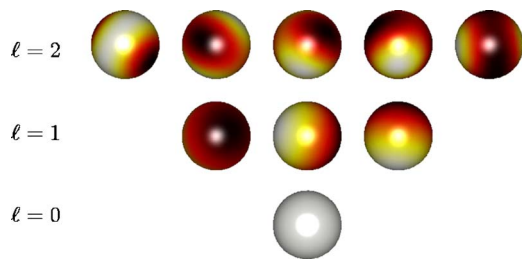


FIG. 3. (Color online) Surface plasmon eigenmodes as computed within our nonretarded approach for a spherical nanoparticle described by the Drude-like dielectric function (8) (see Table I for the corresponding material parameters). The energies of the one-, three-, and fivefold degenerate states are 0 ($\ell=0$), 2.3823 ($\ell=1$), and 2.4815 eV ($\ell=2$), and the corresponding eigenfunctions are given by the spherical harmonics $Y_{\ell m}(\theta, \phi)$.

for an incident light wave with polarization along y (see insets of figure). We emphasize that this approach is based on the full solutions of Maxwell's equations, which naturally incorporates effects of retardation and radiation damping. The arrows in the figure indicate the plasmon energies obtained from the nonretarded calculations, which perfectly coincide with the maxima for the smallest particles. With increasing particle size, the maxima shift to the red and the

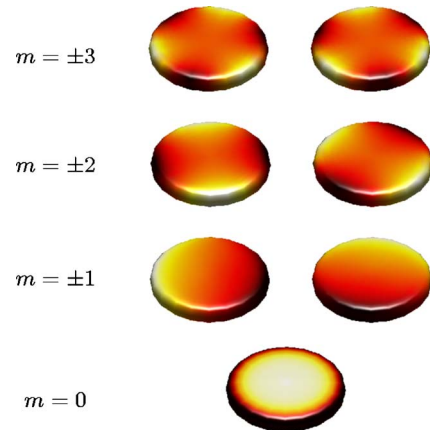


FIG. 4. (Color online) Same as Fig. 3, but for a cylinder with a diameter-to-height ratio of 6:1. The eigenenergies are 0.4162 ($m=0$), 1.8241 ($m=\pm 1$), 2.0902 ($m=\pm 2$), and 2.2279 eV ($m=\pm 3$), and the eigenstates depict the expected cylinder symmetry. Here, the angular part of the plasmon eigenfunctions is given by $e^{\pm im\phi}$; the states with $m=\pm 1$ correspond to dipoles oriented along x and y , and the states with $m=\pm 2$ to quadrupoles. The lowest eigenvalues for an ellipsoid with the same diameter-to-height ratio are 0.2972, 1.7155, 1.9297, and 2.0423 eV, i.e., the energies are redshifted with respect to those of our cylinderlike particles.

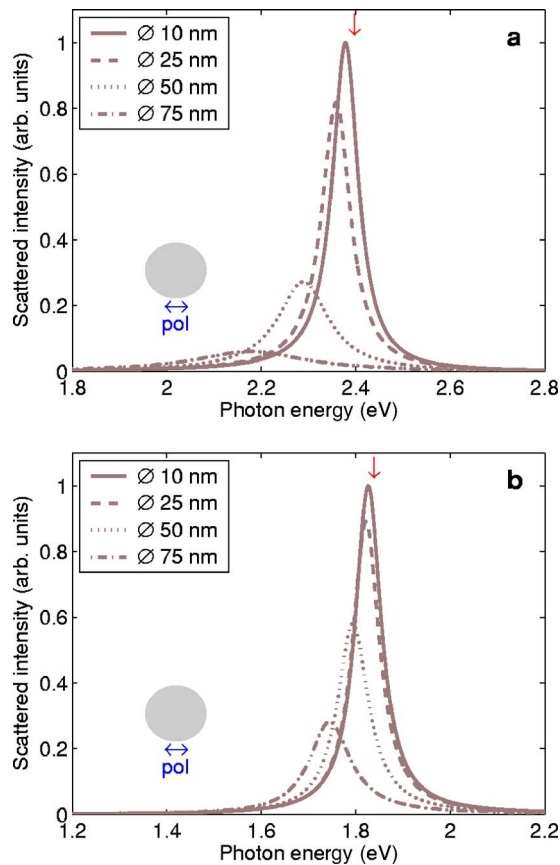


FIG. 5. (Color online) Scattering cross sections for (a) spheres and (b) cylinders, as computed within our retarded approach (Sec. II B) and using the dielectric function (8). The different curves correspond to nanoparticles with different diameter \varnothing , and the arrows indicate the plasmon energies computed within our nonretarded approach. To compensate for the usual $\Omega^2 k^4$ dependence of the cross section, we have scaled all curves with the inverse square volume $1/\Omega^2$ of the nanoparticles.

peaks become further broadened because of radiation damping.

Finally, to demonstrate the versatility of our scheme in Fig. 6 we show the plasmon eigenmodes for a cubiclike particle (other particle shapes with different or lower symmetry, such as, e.g., triangular prisms,^{33,34} could be studied equally well). Such particles were theoretically analyzed by Fuchs²⁵ for ionic crystals, e.g., NaCl, and have recently received increasing interest after demonstration of shape-controlled synthesis of monodisperse samples of silver nanocubes.³⁵ To avoid problems regarding diverging surface charge distributions at the sharp edges and corners of the cube we have rounded them off, in accordance to the actual shape of such nanoparticles.³⁵ The lowest row of Fig. 6 shows the plasmon eigenmode with energy close to zero, which corresponds to the charge distribution of a charged nanocube. The eigenmodes in the middle and upper row with energies close to 2.2 eV are those that can be probed optically. As discussed in length in Ref. 25, only few of these modes have a substantial oscillator strength in the optical far field. Figure 7 shows the optical spectra for a 50-nm Au or Ag nanocube, as obtained within our nonretarded approach using either the Drude di-

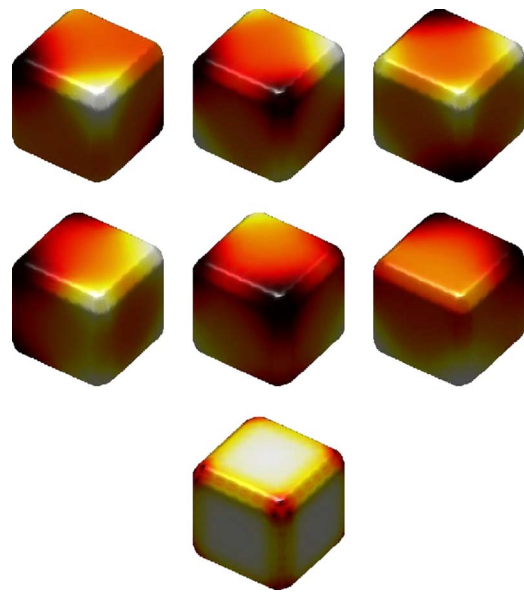


FIG. 6. (Color online) Same as Fig. 3, but for a cubiclike nanoparticle with round edges (the surface is approximated by a set of 2400 triangles). The eigenmodes in the lowest, middle, and upper row have energies of 0, 2.2206, and 2.2595 eV, respectively. For the Drude parameter $\epsilon_0=3.7$ and $\gamma_0^{-1}=36$ fs representative for silver we obtain energies of 0, 2.8155, and 2.8960 eV, respectively.

electric function (solid lines) or that of Johnson and Christy²⁸ (JC). A comparison of the results obtained with these different dielectric functions shows that for Au the Drude framework properly accounts for the peak position but somewhat underestimates the peak width, which is attributed to the lack of d -band damping in the Drude function (8) for photon energies above 2 eV. In contrast, for Ag the Drude and JC dielectric function coincide within a larger range of photon energies, and consequently the results of the Drude and JC framework in Fig. 7 are in almost perfect agreement.

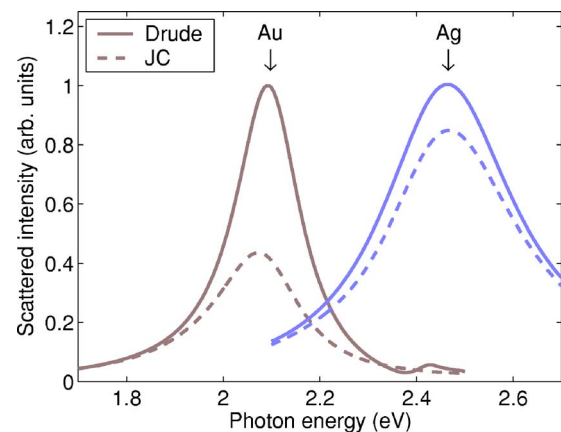


FIG. 7. (Color online) Same as Fig. 5 but for a 50-nm cubic nanoparticle, and for gold and silver (Drude parameters of $\epsilon_0=3.7$ and $\gamma_0^{-1}=36$ fs). The solid lines show results for the Drude dielectric function (8), and the dashed lines for the dielectric function of Johnson and Christy (Ref. 28) (JC).

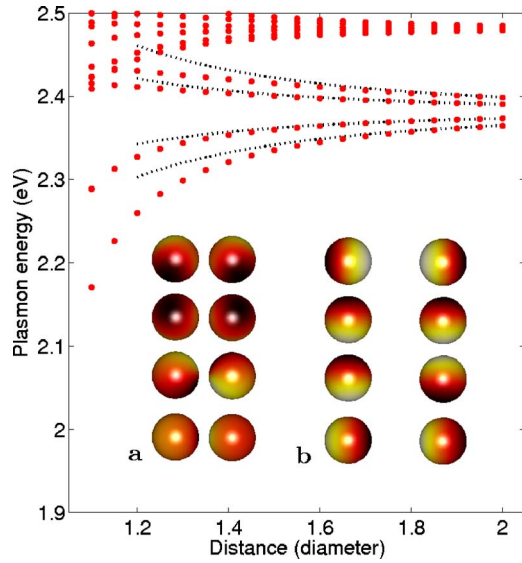


FIG. 8. (Color online) Energies of the plasmon eigenenergies of coupled spherical nanoparticles as a function of interparticle distance, as computed within our nonretarded boundary integral method approach. All distances are measured in units of the sphere diameters. The insets report the plasmon eigenmodes of lowest energy, and for interparticle distances of (a) $d=1.2$ and (b) $d=2$. For $d=2$, these modes correspond, in order of increasing energy, to dipole orientations $\rightarrow\rightarrow$, $\uparrow\downarrow$, $\uparrow\uparrow$, and $\leftarrow\leftarrow$ (note that we do not show the degenerate modes for $\uparrow\downarrow$ and $\uparrow\uparrow$, whose dipole moments are oriented along y rather than z). The dotted lines correspond to the simple expression (15) for the splitting due to a dipole-dipole coupling, and for the dipole orientations depicted in the insets. In the optical far field, only states $\rightarrow\rightarrow$ and $\uparrow\uparrow$ couple to the light.

C. Coupled nanoparticles

When two nanoparticles come close to each other, their plasmon modes couple and, as a result, shift in energy. Within our computational approach, coupled nanoparticles can be simply described by replacing the boundary $\partial\Omega$ of one particle by the (disjoint) boundaries of two particles, whose center coordinates are displaced by the particle distance. All pertinent quantities can then be computed in the same manner as for a single particle. Indeed, neither in the derivation of the retarded¹⁸ nor of the nonretarded¹⁵ boundary integral method is any assumption made about the connectivity of the surface.

Figure 8 shows the lowest surface plasmon eigenenergies for coupled spherical nanoparticles as a function of interparticle distance (see, e.g., Ref. 36 for the description of such coupling within the framework of the extended Mie theory). We observe that, due to coupling and the resulting lowering of spherical symmetry, the degenerate eigenvalues become split. The insets report the plasmon eigenmodes of lowest energy for selected interparticle distances. These modes correspond to different orientations of the dipoles induced in the respective nanoparticles, i.e., $\rightarrow\rightarrow$, $\uparrow\downarrow$, $\uparrow\uparrow$, and $\leftarrow\leftarrow$, in order of increasing energy (dipole modes within an eigenvalue approach for polarizable nanosystems are discussed in some length in Ref. 37). The dipole-dipole interaction energy W_{12} of two dipoles \mathbf{d}_1 and \mathbf{d}_2 located at positions \mathbf{r}_1 and \mathbf{r}_2 is given by¹⁵

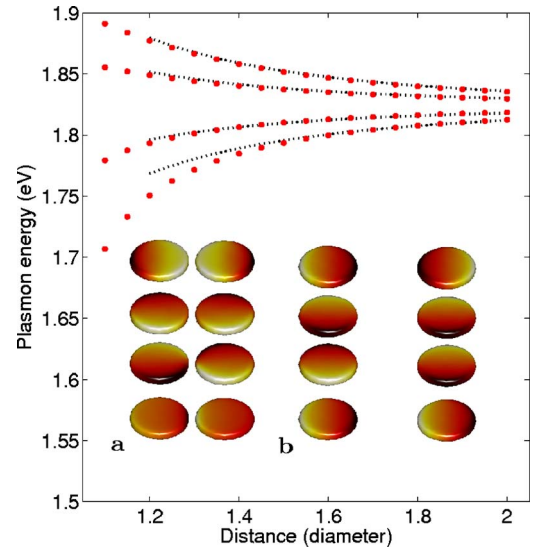


FIG. 9. (Color online) Same as Fig. 8, but for cylinders and for interparticle distances of (a) $d=1.1$, (b) $d=2$ in units of the particle diameter.

$$W_{12} = \frac{\mathbf{d}_1 \cdot \mathbf{d}_2 - 3(\hat{\mathbf{e}} \cdot \mathbf{d}_1)(\hat{\mathbf{e}} \cdot \mathbf{d}_2)}{|\mathbf{r}_1 - \mathbf{r}_2|^3}, \quad (15)$$

where $\hat{\mathbf{e}}$ is the unit vector in the direction $\mathbf{r}_1 - \mathbf{r}_2$. Indeed, the dotted lines in the figure clearly show that the simple expression (15) nicely accounts for the coupling-induced energy splitting within a wide range of interparticle distances. Only at the smallest distances Eq. (15) can no longer describe the splittings, which is attributed to the increasing contribution of higher moments in the charge distributions. A closer inspection of the plasmon eigenmodes reveals that here the distributions on the spheres are distorted such that those parts where the two spheres are charged oppositely move closer towards each other, thus resulting in a lowering of Coulomb energy. At the smallest distances, the states formed from the $\ell=1$ and $\ell=2$ plasmon modes for isolated spheres (Fig. 3) cross, and coupled quadrupole states become lower in energy than coupled dipole states. Figure 9 shows that our findings also prevail for cylindrical nanoparticles, with the only difference that all plasmon modes become nondegenerate as a result of coupling.

Finally, in Fig. 10 we show spectra for coupled (a) spheres and (b) cylinders with diameters of 10 nm and different interparticle distances, as computed within our retarded approach. The solid and dashed curves correspond to light polarizations along x and y , respectively (see insets). We observe two main peaks, associated to the optically allowed coupled $\rightarrow\rightarrow$ and $\uparrow\uparrow$ plasmon modes, which are energetically red- and blueshifted with respect to the single-particle resonances depicted in Fig. 5. With decreasing distance the energy splitting of the two plasmons increases because of the enhanced Coulomb coupling. For larger particles we find, similarly to the single-particle case, a redshift of both peaks, a reduction of the peak splittings, and a further broadening because of radiation damping. Further details as

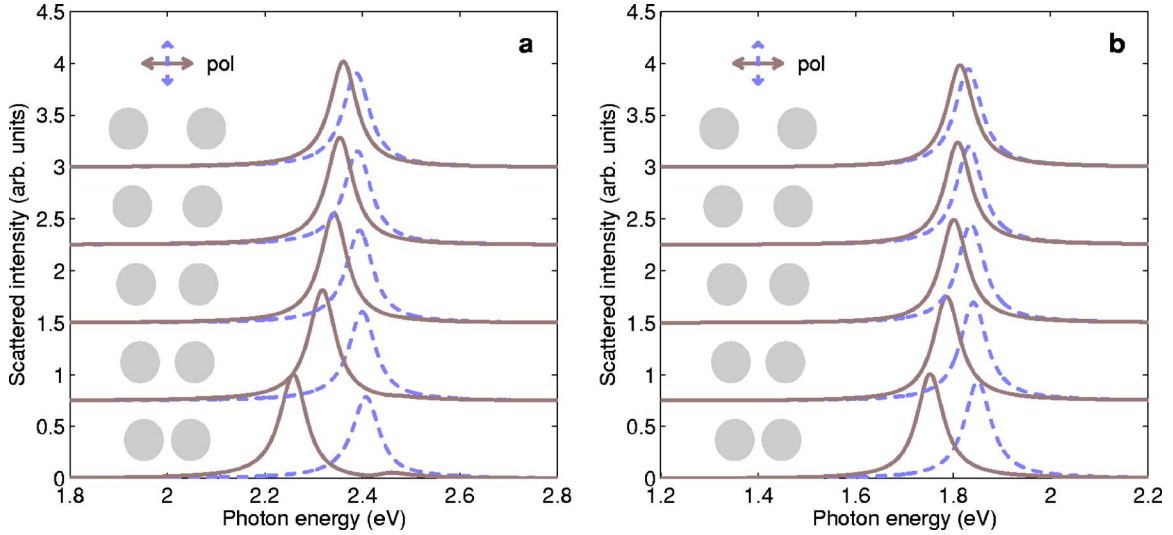


FIG. 10. (Color online) Scattering cross sections for coupled (a) spheres and (b) cylinders with a diameter of 10 nm, as computed within our retarded approach (Sec. II B) and using the dielectric function (8). The different curves correspond to different interparticle distances of 12, 14, 16, 18, 20 nm, and are offset for clarity. The solid and dashed lines correspond to x and y polarization of the incident light, as indicated in the inset.

well as a direct comparison with experiment will be published elsewhere.

IV. CONCLUSIONS

In conclusion, we have employed the boundary integral method for the calculation of plasmon resonances in single and coupled metallic nanoparticles of arbitrary shape. For the solution of the full Maxwell equations (retarded case) we have adopted an indirect method,^{17,18} and for the static limit suited for small nanoparticles (nonretarded case) we have used the direct method. In the latter approach, we have shown that a Drude description for the dielectric function allows to formulate an eigenvalue problem for the electron dynamics in the metal, whose solutions directly provide the surface plasmon resonances. This approach has been used to compute eigenmodes for spherical, cylindrical, and cubic nanoparticles, and to discuss the role of interparticle coupling. Over a wide range of distances the simple dipole-dipole coupling has been shown to provide an excellent description for interparticle couplings, and only at the smallest distances significant deviations have been found. We have used the retarded approach to investigate effects of retardation and radiation damping, which have been demonstrated to be of importance for larger nanoparticles.

APPENDIX

In this appendix we show how to derive the equation of motion (9) for the surface charge density within the framework of the jellium (or hydrodynamic)^{38,39} model. Our starting point is given by the Boltzmann equation for the electrons,

$$\frac{\partial f}{\partial t} + \mathbf{v} \cdot \nabla_{\mathbf{r}} f + \mathbf{F} \cdot \nabla_{\mathbf{v}} f = \left(\frac{\partial f}{\partial t} \right)_{\text{coll}}, \quad (\text{A1})$$

with $f(\mathbf{r}, \mathbf{v}, t)$ the electron distribution function, \mathbf{v} the velocity, and \mathbf{F} the Lorentz force acting on the particles. Here, the

left-hand side accounts for the drift and force contributions, and the right-hand side for electron collisions. A more simplified description scheme can be obtained by introducing the moments of f through

$$n(\mathbf{r}, t) = - \int d\mathbf{v} f(\mathbf{r}, \mathbf{v}, t), \quad (\text{A2a})$$

$$\mathbf{j}(\mathbf{r}, t) = - \int d\mathbf{v} \mathbf{v} f(\mathbf{r}, \mathbf{v}, t), \quad (\text{A2b})$$

with n and \mathbf{j} the charge and current density, respectively, and the minus sign accounting for the negative electron charge. Higher moments, such as the kinetic stress tensor,⁴⁰ will be neglected. Performing such moment expansion in Eq. (A1) and truncating at the level of n and \mathbf{j} readily yields

$$\frac{\partial n}{\partial t} + \nabla \cdot \mathbf{j} = 0, \quad (\text{A3a})$$

$$\frac{\partial \mathbf{j}}{\partial t} + \mathbf{E} n + \frac{\mathbf{j}}{c} \times \mathbf{B} = \left(\frac{\partial \mathbf{j}}{\partial t} \right)_{\text{coll}}, \quad (\text{A3b})$$

where the last term on the right-hand side accounts for scattering processes. Equations (A3a) and (A3b) are known as the continuity and force equation, respectively.^{15,40}

The equilibrium state of the metal nanoparticles is a constant electron density n_0 , whereby the field produced by n_0 is precisely canceled by that of the positive jellium background. When the particles are subject to an external perturbation, this density will be modified and a current will be induced. Expanding Eq. (A3b) in terms of the modified density n (we use for simplicity the same symbol), the induced current \mathbf{j} , and the electric field \mathbf{E} , and keeping only lowest-order terms, then gives together with the continuity equation

$$\frac{\partial^2 n}{\partial t^2} - n_0 \nabla \cdot \mathbf{E} - \mathbf{E} \cdot \nabla n_0 + \nabla \cdot \left(\frac{\partial \mathbf{j}}{\partial t} \right)_{\text{coll}} = 0. \quad (\text{A4})$$

Here, \mathbf{E} is the sum of the external and induced electric field, the latter being the solution of the Poisson equation for the induced charge n . We next follow Ref. 41 and split the density $n = n_v + \sigma$ into a volume and surface part n_v and σ , respectively. Using $\nabla n_0 = -n_0 \hat{\mathbf{n}}$, with $\hat{\mathbf{n}}$, the outer surface normal, and performing a Fourier transform in time, we obtain

$$\omega(\omega + i\gamma_0)n_v - n_0 \nabla \cdot \mathbf{E} = 0, \quad (\text{A5a})$$

$$\omega(\omega + i\gamma_0)\sigma + n_0 \hat{\mathbf{n}} \cdot \mathbf{E} = 0, \quad (\text{A5b})$$

where we have lumped all collision effects into the relaxation rate γ_0 . It is easy to show¹⁵ that the solutions of Eq. (A5a) and (A5b) are precisely those of Maxwell's equations with the Drude dielectric function (8). For simplicity we shall neglect below the volume part n_v .⁴¹

The electric field \mathbf{E} in Eq. (A5b) can be decomposed into an external and induced part \mathbf{E}_{ext} and \mathbf{E}_{ind} , respectively. The

latter is the solution of the Poisson equation, which, in the nonretarded limit, can be obtained by means of the scalar potential ϕ . From Eq. (A5b) we observe that the quantity needed in the calculation of σ is the normal component $\hat{\mathbf{n}} \cdot \mathbf{E}_{\text{ind}} = -\phi'_{\perp}$ of the induced field at the metal boundary $\partial\Omega$, where $\phi'_{\perp} = \hat{\mathbf{n}} \cdot \nabla \phi$ denotes the surface derivative of ϕ . The subscript is a reminder that the derivative has to be taken inside the particle within which the electrons are confined.

We next use the boundary integral equation (4) to relate ϕ'_{\perp} to the surface charge σ . With $\hat{\mathbf{n}} = \hat{\mathbf{n}}_1$ the outer surface normal of the metal and $\phi'_{\perp} = \hat{\mathbf{n}} \cdot \nabla \phi$ the outer surface derivative, we obtain from Eq. (4)

$$2\pi\phi = \pm(G\phi'_{\perp,2} - F\phi), \quad (\text{A6})$$

with $F(s, s') = -\hat{\mathbf{n}} \cdot (\mathbf{s} - \mathbf{s}') / (|\mathbf{s} - \mathbf{s}'|)^3$ the surface derivative of the Green function. Together with the boundary condition $\hat{\mathbf{n}} \cdot (\mathbf{D}_2 - \mathbf{D}_1) = 4\pi\sigma$ for the dielectric displacement we find after some straightforward manipulations the desired expression (9).

*Electronic address: ulrich.hohenester@uni-graz.at

¹U. Kreibig and M. Vollmer, in *Optical Properties of Metal Clusters*, edited by U. Gonser, R. M. Osgood, Jr., M. B. Panish, and H. Sakaki, Springer Series in Material Science Vol. 25 (Springer, Berlin, 1995).

²M. Moskovits, *Rev. Mod. Phys.* **57**, 783 (1985).

³G. C. Schatz and R. P. V. Duyne, in *Handbook of Vibrational Spectroscopy*, edited by J. M. Chalmers and P. R. Griffiths (Wiley, New York, 2001), 759-774.

⁴A. Haes and R. P. V. Duyne, *J. Am. Chem. Soc.* **124**, 10596 (2002).

⁵M. Quinten, A. Leitner, J. R. Krenn, and F. R. Aussenegg, *Opt. Lett.* **23**, 1331 (1998).

⁶W. Rechberger, A. Leitner, A. Hohenau, J. R. Krenn, and F. R. Aussenegg, *Opt. Commun.* **220**, 137 (2003).

⁷L. Gunnarson, T. Rindzevicius, J. Prikulis, B. Kasemo, M. Käll, S. Zou, and G. C. Schatz, *J. Phys. Chem. B* **109**, 1079 (2005).

⁸K. S. Yee, *IEEE Trans. Antennas Propag.* **14**, 302 (1966).

⁹A. J. Ward and J. B. Pendry, *J. Mod. Opt.* **43**, 773 (1995).

¹⁰A. J. Ward and J. B. Pendry, *Comput. Phys. Commun.* **128**, 590 (2000).

¹¹O. J. F. Martin, C. Girard, and A. Dereux, *Phys. Rev. Lett.* **74**, 526 (1995).

¹²M. Paulus, P. Gay-Balmaz, and O. J. F. Martin, *Phys. Rev. E* **62**, 5797 (2000).

¹³M. S. Tomaš, *Phys. Rev. A* **51**, 2545 (1995).

¹⁴J. P. Kottmann and O. J. F. Martin, *IEEE Trans. Antennas Propag.* **48**, 1719 (2000).

¹⁵J. D. Jackson, *Classical Electrodynamics* (Wiley, New York, 1962).

¹⁶T. Søndergaard and B. Tromborg, *Phys. Rev. B* **66**, 155309 (2002).

¹⁷F. J. Garcia de Abajo and A. Howie, *Phys. Rev. Lett.* **80**, 5180 (1998).

¹⁸F. J. Garcia de Abajo and A. Howie, *Phys. Rev. B* **65**, 115418 (2002).

¹⁹S. Amini and S. M. Kirkup, *J. Comput. Phys.* **118**, 208 (1995).

²⁰A. J. Burton and G. F. Miller, *Proc. R. Soc. London, Ser. A* **323**, 201 (1971).

²¹G. D. Mahan, *Many-Particle Physics* (Plenum, New York, 1981).

²²I. A. Larkin and M. I. Stockman, *Nano Lett.* **5**, 339 (2005).

²³M. Brack, *Rev. Mod. Phys.* **65**, 677 (1993).

²⁴J. Aizpurua, G. W. Bryant, L. J. Richter, F. J. Garcia de Abajo, B. K. Kelley, and T. Mallouk, *Phys. Rev. B* **71**, 235420 (2005).

²⁵R. Fuchs, *Phys. Rev. B* **11**, 1732 (1975).

²⁶F. Ouyang and M. Isaacson, *Philos. Mag. B* **60**, 481 (1989).

²⁷F. Ladstädter, U. Hohenester, P. Puschnig, and C. Ambrosch-Draxl, *Phys. Rev. B* **70**, 235125 (2004).

²⁸P. B. Johnson and R. W. Christy, *Phys. Rev. B* **6**, 4370 (1972).

²⁹Note that for conceptual clarity we have introduced the symbols ϵ_0 and ϵ_b for the real-valued dielectric constants, instead of the previous notations ϵ_1 and ϵ_2 for the generally complex-valued dielectric functions.

³⁰C. B. Barber, D. P. Dobkin, and H. T. Huhdanpaa, *ACM Trans. Math. Softw.* **22**, 469 (1996).

³¹I. H. Sloan and R. S. Womersley, *J. Comput. Appl. Math.* **149**, 227 (2002).

³²This is attributed to our use of an optimized set of points for the sphere triangulation (Ref. 31). More simplified discretization schemes, such as an equidistant one, turned out to give slightly larger deviations.

³³E. Hao and C. Schatz, *J. Chem. Phys.* **120**, 357 (2004).

³⁴D. A. Stuart, A. J. Haes, C. R. Yonzon, E. M. Hicks, and R. P. Van Duyne, *IEE Proc. Nanobiotechnol.* **152**, 13 (2005).

³⁵Y. Sun and Y. Xia, *Science* **298**, 2176 (2002).

³⁶D. J. Bergman, *Phys. Rev. B* **19**, 2359 (1979).

³⁷P. B. Allen, *J. Chem. Phys.* **120**, 2951 (2004).

³⁸R. H. Ritchie, *Prog. Theor. Phys.* **29**, 607 (1963).

³⁹R. H. Ritchie and R. E. Wilems, *Phys. Rev.* **178**, 372 (1969).

⁴⁰K. S. Singwi and M. P. Tosi, *Solid State Phys.* **36**, 177 (1981).

⁴¹J.-P. Connerade and A. V. Solov'yov, *Phys. Rev. A* **66**, 013207 (2002).